doi:10.1016/j.jmb.2004.11.003 J. Mol. Biol. (2005) 345, 651–658

JMB

Available online at www.sciencedirect.com

SCIENCE DIRECT®

ELSEVIER

COMMUNICATION

Mapping the Binding of the N-terminal Extracellular Tail of the CXCR4 Receptor to Stromal Cell-derived Factor-1α

Elliott K. Gozansky, John M. Louis, Michael Caffrey and G. Marius Clore*

Laboratory of Chemical Physics National Institute of Diabetes and Digestive and Kidney Disease, National Institutes of Health, Bethesda, MD 20892-0520, USA

**Corresponding author*

The solution structure of monomeric stromal cell-derived factor-1α (SDF-1α), the natural ligand for the CXCR4 G-coupled receptor, has been solved by multidimensional heteronuclear NMR spectroscopy. The structure has a characteristic chemokine fold and is in excellent agreement with the individual subunits observed in the crystal structures of dimeric SDF-1α. Using various peptides derived from the N-terminal extracellular tail of the CXCR4 receptor, we show that the principal determinants of binding reside in the N-terminal 17 residues of CXCR4, with a major contribution from the first six residues. From $^{15}N/^{1}H_N$ chemical shift pertubation studies we show that the interaction surface on SDF-1α is formed by the undersurface of the three-stranded antiparallel β-sheet bounded by the N-terminal loop on one side and the C-terminal helix on the other. This surface overlaps with but is not identical to that mapped on several other chemokines for the binding of equivalent peptides derived from their respective receptors.

Keywords: chemokine; SDF-1α; CXCR4 receptor; chemical shift mapping; solution structure

The chemokines comprise a large superfamily of cytokines that are involved in chemotaxis and pro-activation of leukocytes.[1] All chemokines (with the exception of lymphotactin) possess two disulfide bridges and the superfamily has been divided into several classes, CC, CXC and CX_3C, depending upon the separation between the first two cysteine residues.[1] Chemokines within each family share a high degree of sequence similarity and a similar spectrum of biological specificities. Stromal cell-derived factor-1α (SDF-1α)[2,3] is an unusual member of the CXC family in that its sequence is equally divergent from both the CXC and CC chemokines, with average sequence identities of only 20–25%.[4] The natural and exclusive ligand for SDF-1α is the CXCR4 G-coupled receptor, which is also the co-receptor involved in HIV-1 envelope-mediated cell fusion by T-tropic strains of HIV-1.[5,6] SDF-1α displays chemo-attractant activity for lymphocytes and monocytes, plays an important role in trafficking, export and homing of bone marrow cells, inhibits infection by T-tropic strains of HIV-1, and is involved in the spread of leukemias to multiple marrow sites and in regulating metastasis of a number of solid tumors, including sarcomas and prostate cancer.[7,8]

The solution NMR structure of monomeric SDF-1α, determined principally using two-dimensional homonuclear methods, was first reported by Crump *et al.*,[4] followed by two independent crystal structures of dimeric SDF-1α.[9,10] While the overall topologies of the NMR and crystal structures are the same, significant differences are apparent, particularly with respect to the orientation of the C-terminal helix, which differs by approximately 35° between the solution and crystal structures. To resolve this issue and ascertain whether the discrepancy is due to the multimeric state of SDF-1α, we first carried out an independent structure determination by multidimensional NMR spectroscopy. Using $^{1}H–^{15}N$ correlation spectroscopy we then analyzed the binding of various peptides derived from the N-terminal extracellular tail of the

Present addresses: E. K. Gozansky, University of Michigan Medical School, Ann Arbor, MI 48109, USA; M. Caffrey, Department of Biochemistry and Molecular Genetics, University of Illinois at Chicago, IL 60607, USA.

Abbreviations used: SDF-1α, stromal cell-derived factor-1α; NOE, nuclear Overhauser effect.

E-mail address of the corresponding author: mariusc@intra.niddk.nih.gov

0022-2836/$ - see front matter Published by Elsevier Ltd.

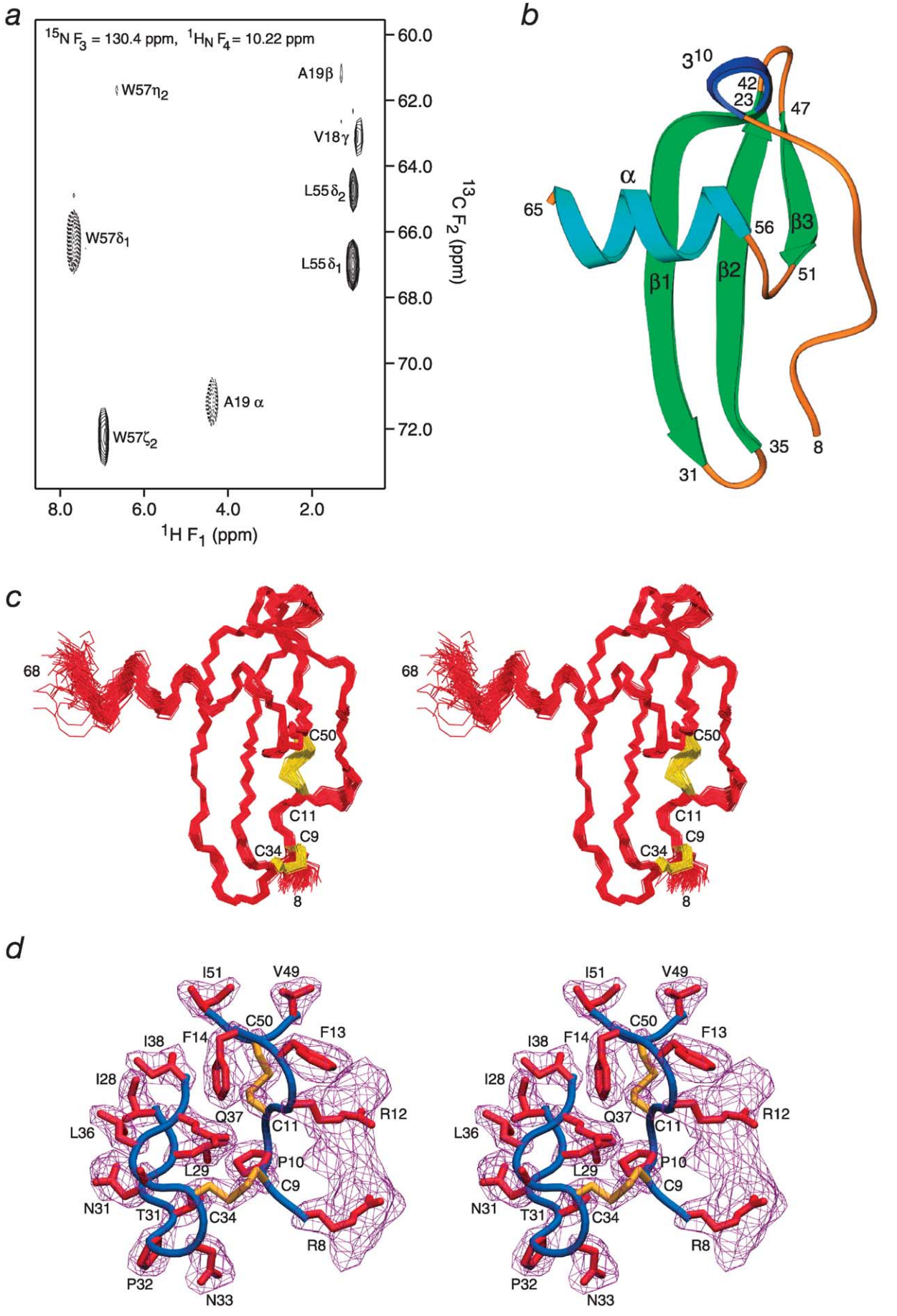

Figure 1 (*legend opposite*)

CXCR4 receptor to dissect some of the determinants involved in the interaction of CXCR4 with SDF-1α and to map the interaction surface on SDF-1α.

In solution SDF-1α exists as an equilibrium mixture of monomeric and dimeric forms that is sensitive to both pH and solute concentration, as assessed by ^{1}H–^{15}N correlation spectroscopy. At pH 6.8 (near neutral) and 35 °C, exchange between the two forms is slow to intermediate on the chemical shift scale with extensive line broadening. As the sample concentration is increased, the emergence of new, low intensity peaks, attributable to the dimeric form is observed from which we calculate an equilibrium dimerization constant of 290 M^{-1} and an exchange lifetime of $<885\ s^{-1}$. The low dimerization constant at neutral pH suggests that the physiologically relevant form of SDF-1α is the monomer. At pH 5.5 or less, SDF-1α exists entirely in the monomeric form in agreement with previously published data.[4] All structural studies were therefore performed at pH 5.5.

The solution structure of SDF-1α was re-determined independently by multidimensional NMR spectroscopy[11] on the basis of 1029 experimental NMR restraints. A description of the experimental NMR and structure calculation methods is provided in the legend to Figure 1 and a summary of the structural statistics is given in Table 1. An example of the quality of the nuclear Overhauser effect (NOE) data is illustrated in Figure 1 by a plane taken from the 4D $^{13}C/^{15}N$-separated NOE spectrum. The global fold of SDF-1α is displayed in Figure 1(b), a best-fit superposition of the backbone of the 100 final simulated annealing structures is shown in Figure 1(c), and an example of the quality with which the side-chain coordinates have been determined is provided by the re-weighted atomic density probability map[12] depicted in Figure 1(d). The high precision with which the backbone coordinates have been determined (cf. Figure 1(b) and Table 1) is a result of the combined impact of the NOE-derived distance, torsion angle, backbone

Figure 1. Structure of SDF-1α. (a) Example of a $^{1}H(F_1)/^{13}C(F_2)$ plane from the 4D $^{13}C/^{15}N$-separated NOE spectrum (mixing time = 120 ms) taken at $^{15}N(F_3) = 130.4$ ppm/$^{1}HN(F_4) = 10.22$ ppm, which corresponds to the $N^{\varepsilon 1}H$ of Trp57. (Note that extensive folding was employed for $^{13}C(F_2)$ dimension which was recorded with a sweep width of 20.71 ppm; peaks folded an even number of times have positive contours, shown by continuous lines, while peaks folded an odd number of times have negative contours shown by broken lines; thus, for example, the absolute ^{13}C shift of Leu55δ1 is at 25.5 ppm). (b) Ribbon drawing of the restrained regularized mean structure of SDF-1α (green, β-sheet; cyan, helix; dark blue, 3_{10} helix; and brown, loops). (c) Backbone (N, C^{α}, C atom) best-fit superposition of the final 100 simulated annealing structures (red) with the two disulfide bridges shown in yellow. (Residues 1–7 are not shown since they are disordered in solution.) (d) Isosurface of the re-weighted atomic density map (purple) for selected side-chains drawn at a value of 20% maximum,[12] calculated from the 100 simulated annealing structures; the backbone of the restrained regularized mean structure is shown as a blue tube and side-chain coordinates within the atomic density map are shown in red. Note that the atomic density map for Arg8 and Arg12 clearly indicates that these two side-chains occupy multiple rotameric states. SDF-1α with an additional three residues (Ser-Asp-Gly) at the N terminus was cloned into the pET11a vector and expressed in *Escherichia coli* BL-21(DE3). Cells were grown at 37 °C in minimal medium with $^{15}NH_4Cl$ and/or $13C_6$-glucose as the sole nitrogen and carbon sources, respectively. Cells derived from 1 l of culture were suspended in 80 ml of buffer A (50 mM Tris–HCl (pH 8), 10 mM EDTA, 10 mM dithiothreitol (DTT)]), followed by the addition of lysozyme (100 μg/ml) and sonicated at 4 °C. The insoluble recombinant protein was washed by resuspension in 70 ml of buffer containing 50 mM Tris–HCl (pH 8), 10 mM EDTA, 10 mM DTT and 2 M urea and subsequently in buffer A. The insoluble fraction was pelleted by centrifugation at 20,000*g* for 30 minutes at 4 °C. The final pellet was solubilized in 50 mM Tris–HCl (pH 8.0), 7.5 M guanidine–HCl, 5 mM EDTA, 100 mM DTT to yield a protein concentration of ~20 mg/ml. 30 mg of protein was applied on a Superdex-75 column (HiLoad 2.6 cm × 60 cm, GE Healthcare, NJ) equilibrated in 50 mM Tris–HCl (pH 8), 4 M guanidine–HCl, 5 mM EDTA, 5 mM DTT, and eluted at a flow-rate of 3 ml/minute at ambient temperature. Peak fractions were pooled and ~12 mg (0.25 mg/ml) of protein in the column buffer was folded at room temperature against 4 l of buffer in three steps: first against 1 M guanidine–HCl, 50 mM Tris–HCl (pH 8), 50 mM NaCl, 5 mM EDTA overnight and then twice against 20 mM Tris–HCl (pH 8), 0.1 M NaCl for 5–6 hours. The protein was concentrated to ~2 ml and applied on a Superdex-75 column (HiLoad 2.6 cm × 60 cm) in 50 mM sodium phosphate buffer (pH 4.8). Peak fractions eluting at a retention volume between 200 ml and 225 ml corresponding to the monomeric folded SDF-1α were pooled and concentrated. Samples for NMR contained ~1 mM protein in 50 mM phosphate buffer (pH 5.5). All NMR experiments were carried out at 35 °C on Bruker DMX500 and DMX600 spectrometers. Spectra were analyzed using the programs PIPP, CAPP and STAPP.[22] Assignment was carried out using 3D double and triple resonance experiments (HNCACB, HNCO, CBCA(CO)NH, C(CCO)NH, H(CCO)NH, HCCH-COSY, HCCH-TOCSY).[11] NOE distance restraints (1.8–2.7 Å, 1.8–3.5 Å, 1.8–5.0 Å and 1.8–6.0 Å, corresponding to strong, medium, weak and very weak NOE cross-peak intensities) were derived from 3D ^{15}N-separated and ^{13}C-separated NOE experiments and 4D $^{13}C/^{15}N$-separated and $^{13}C/^{13}C$-separated NOE experiments.[11] Three-bond *J* couplings ($^{3}J_{HNH\alpha}$, $^{3}J_{NC\gamma}$, $^{3}J_{C'C\gamma}$ and $^{3}J_{C\alpha C\delta}$ couplings) were measured using quantitative *J* correlation spectroscopy.[23] Side-chain torsion angle restraints were derived from ^{3}J couplings combined with information from the NOE data.[11] $^{1}D_{NH}$ residual dipolar couplings were obtained from the difference in $^{1}J_{HN}$ couplings measured in liquid crystalline (5% bicelles, 3 : 1 DMPC:DHPC) medium and in isotropic (water) medium.[24] Backbone ϕ/ψ torsion angle restraints were derived from backbone chemical shifts using the program TALOS.[25] The structures were calculated using well-established procedures[26] from the experimental restraints by simulated annealing in torsion angle space[27] using the program Xplor-NIH.[28] The non-bonded contacts in the target function were represented by a quartic van der Waals repulsion term[24] supplemented by torsion angle[13] and hydrogen-bonding[14] database potentials of mean force, and a radius of gyration restraint to ensure optimal packing.[29] Structure Figures were generated with the programs VMD-XPLOR[30] and RIBBONS.[31] Reweighted atomic density probability maps (contoured at 20% of maximum value) were calculated from the ensemble of simulated annealing structures as described.[12]

Table 1. Structural statistics

	⟨SA⟩	$(\bar{S}A)_r$
r.m.s deviations from experimental NMR restraints		
Distance restraints (Å) (620)	0.015±0.002	0.010
Torsion angle restraints (deg.) (202)	0.37±0.10	0.45
$^3J_{HN\alpha}$ coupling constants (Hz) (37)	0.79±0.09	0.81
$^{13}C^{\alpha}/^{13}C^{\beta}$ chemical shift restraints (ppm) (135)	1.12±0.04	1.14
$^1D_{NH}$ dipolar coupling *R*-factor (%) (35)[a]	6.2±0.8	5.5
Deviations from idealized covalent geometry		
Bonds (Å)	0.003±0	0.005
Angles (deg.)	0.45±0	0.60
Improper torsions (deg.)	0.72±0.06	0.62
Ramachandran map analysis[b]		
Most favored region (%)	87.4±2.0	87.7
Additionally allowed region (%)	10.6±2.0	10.5
Generously allowed region (%)	1.8±0.6	1.8
Disallowed region (%)	0.2±0.6	0
Number of bad contacts per 100 residues[b]	8.0±2.1	4.8
Coordinate precision (Å)[c]		
Backbone (N, C^{α}, C, O)	0.42±0.06	
All atoms	0.91±0.12	

The notation of the NMR structures is as follows: <SA> are the final 100 simulated annealing structures. $(\bar{S}A)_r$ is the restrained regularized mean structure derived from the mean coordinates obtained by averaging the coordinates of the 100 simulated annealing structures best-fitted to each other (with respect to residues 8–65). The number of terms for the various restraints is given in parentheses. None of the structures exhibits interproton distance violations >0.3 Å or torsion angle violations >5°. There are 562 structurally useful interproton distance restraints comprising: 174 sequential ($|i-j|=1$), 94 medium-range ($1<|i-j|\leq 5$) and 121 long-range ($|i-j|>5$) restraints, and 173 intraresidue restraints. 58 distance restraints for 29 backbone hydrogen bonds located in helices and sheets were added during the final stages of refinement. The torsion angle restraints comprise 69 ϕ, 55 ψ and 78 side-chain χ restraints.

[a] The dipolar coupling *R*-factor, which scales between 0% and 100% is defined as the ratio of the r.m.s. deviation between observed and calculated values to the expected r.m.s. deviation if the vectors were randomly distributed, given by $[2D_a^2(4+3\eta^2)/5]^{1/2}$, where D_a is the magnitude of the principal component of the alignment tensor and η the rhombicity.[33] The values of D_a^{NH} and η, derived from the distribution of normalized dipolar couplings,[34] are −9.7 Hz and 0.46, respectively.

[b] Calculated with the program PROCHECK.[35] The dihedral angle *G*-factors for ϕ/ψ, χ_1/χ_2, χ_1 and χ_3/χ_4 are −0.24(±0.06), 0.53(±0.08), 0.24(±0.22) and 0.09(±0.18), respectively.

[c] The precision of the coordinates is defined as the average atomic r.m.s. difference between the individual 100 simulated annealing structures and the corresponding mean coordinates obtained by best-fitting residues 8–65. Residues 1–7 and 66–68 are disordered in solution.

NH dipolar coupling, $^3J_{HN\alpha}$ coupling and $^{13}C^{\alpha}/^{13}C^{\beta}$ chemical shift restraints, supplemented by multi-dimensional torsion angle (backbone and side-chain) and hydrogen-bonding database potentials of mean force.[13,14]

The overall fold of SDF-1α is characteristic of the chemokine family of proteins comprising a three-stranded antiparallel β-sheet (residues 23–31, 35–42 and 47–51) in a Greek key arrangement on top of which lies a C-terminal α-helix (residues 56–64) (Figure 1(b)). The long axis of the α-helix is oriented orthogonal to the underlying strands of the β-sheet. Two disulfide bridges, both of which have left-handed spiral conformations, connect the N-terminal extended loop to strands β2 (Cys9–C34) and β3 (Cys11–Cys50). Unlike other CXC chemokines

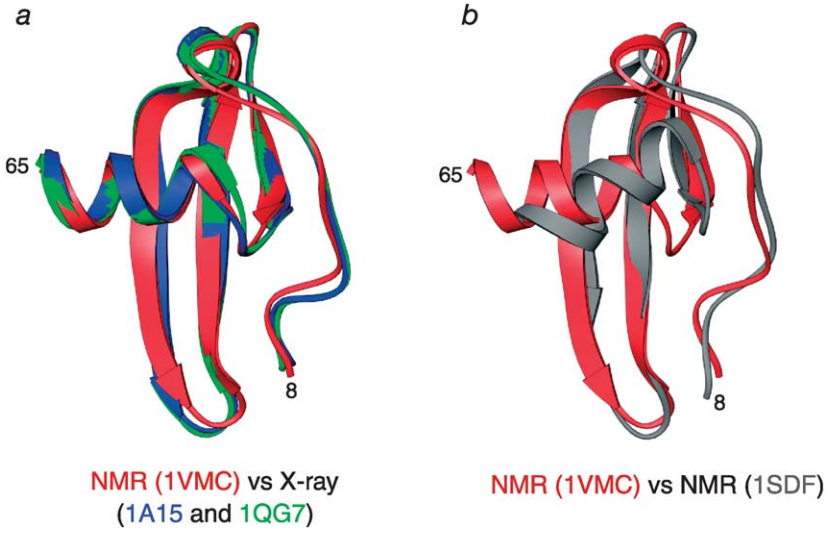

Figure 2. Comparison of the current NMR structure of monomeric SDF-1α (red, labeled as NMR(1VMC)), with (a) the coordinates of one subunit from two independent crystal structures of dimeric SDF-1α solved at resolutions of 2.2 Å (blue, 1A15)[9] and 2.0 Å (green, 1AQG7),[10] and (b) the original monomeric NMR structure (gray, 1SDF) solved by Crump *et al.*[4] Note that the orientation of the helix with regard to the underlying β-sheet in the 1SDF structure differs by ∼35° from that in the other three structures, and the conformation of the loop connecting strand β3 to the helix is significantly different as well.

where the first disulfide bridge has a right-handed hook conformation, both disulfide bridges of SDF-1α adopt the same conformation as that associated with the CC chemokines.[15] This may be due to the presence of a proline residue between Cys9 and Cys11 in SDF-1α. A 3^{10} helix (residues 19–22) immediately precedes strand β1. Residues 1–7 and 66–68 are disordered in solution, as evidenced by the absence of any non-sequential ^{1}H–^{1}H NOEs and low (<0.6) ^{15}N–{^{1}H} heteronuclear NOE values.

A comparison of the current solution NMR structure of SDF-1α with individual subunits from two independently solved crystal structures[9,10] and with the original NMR structure of Crump *et al*.[4] is provided in Figures 2(a) and (b), respectively. The agreement between the present NMR structure and the crystal structures is excellent with a backbone atomic rms difference (residues 8–65) of 0.9 Å between the NMR structure and the two crystal structures, compared to 0.5 Å between the two crystal structures. The orientation of the helix with respect to the β-sheet is the same in all three structures. In contrast, the orientation of the C-terminal helix in the original NMR structure[4] differs by about 35°, there are significant differences in the loop connecting strand β3 and the α-helix, and strands β1 and β2 are two residues shorter (Figure 2(b)). It is possible that these differences arise from the slightly different conditions employed in this study (50 mM sodium phosphate, pH 5.5 buffer) compared to the previous one (20 mM sodium acetate buffer, pH 4.9). Alternatively, the differences may be due to some misclassifications of NOE intensities and/or some NOE misassignments in the earlier study. This is supported by the occurence in the original NMR structure[4] of 35 NOE distance violations greater than 2 Å against the present NOE distance restraints dataset. This is perhaps not surprising given that the original NMR structure was primarily based on homonuclear two-dimensional NOE experiments[4] and side-chain ^{1}H chemical shift overlap for SDF-1α is quite extensive, necessitating the use of multidimensional NMR (cf. the methyl resonances of Leu55, Val18 and Ala19 in Figure 1(a)).

Previous biochemical studies have shown that the N-terminal extracellular tail of CXCR4 is involved in binding SDF-1.[16] We therefore probed the interaction of four peptides comprising residues 1–27, 1–17, 7–27 and 18–27 of the CXCR4 receptor (Figure 3(a)) with ^{15}N-labeled SDF-1α using ^{1}H–^{15}N correlation spectroscopy. The results are displayed in Figure 3. A comparison of the ^{1}H–^{15}N correlation spectrum of ^{15}N-labeled SDF-1α in the absence and in the presence of a 1.5-fold excess of CXCR4$^{1–27}$ is shown in Figure 3(b). The binding of CXCR4$^{1–27}$, CXCR4$^{1–17}$ and CXCR4$^{7–27}$ to SDF-1α is in fast exchange on the chemical shift scale with an exchange rate $\gg 1000\ s^{-1}$. The equilibrium dissociation constants for the binding of CXCR4$^{1–27}$ and CXCR4$^{1–17}$ to SDF-1α, determined from titration experiments, are 45(±10) μM (Figure 3(c)) and 133(±40) μM, respectively. The pattern of chemical shift perturbation induced by CXCR4$^{1–27}$, CXCR4$^{1–17}$ and CXCR4$^{7–27}$ is very similar (Figure 3(d)), although the magnitude of the chemical shift perturbations is largest for CXCR4$^{1–27}$ and smallest for CXCR4$^{7–27}$. Indeed, the binding of CXCR4$^{7–27}$ is too weak to permit the determination of an equilibrium constant. No chemical shift perturbation is observed for CXCR4$^{18–27}$. The absence of any detectable binding for CXCR4$^{18–27}$ together with the observation that the affinity of CXCR4$^{1–17}$ is only threefold lower than that of CXCR4$^{1–27}$ suggests that the principal determinants of binding reside in the N-terminal 17 residues, and that the contribution of residues 18–27 is weak and probably non-specific in nature. The observation that the binding of CXCR4$^{7–27}$ is much reduced relative to CXCR4$^{1–27}$ and CXCR4$^{1–17}$ indicates that the first N-terminal six residues of CXCR4 make the single largest contribution to the binding energy of the N-terminal extracellular tail of CXCR4 to SDF-1α.

The regions with the largest chemical shift perturbations (defined in this instance as $\Delta_{H/N} = [(\Delta\delta^1H)^2 + (\Delta\delta^{15}N)^2]^{1/2} > 40$ Hz upon addition of 1.5 eq of CXCR4$^{1–27}$) comprise a single residue (Phe13) in the N-terminal loop, residues at the N-terminal end of strand β1 (Val23, Lys24, His25), the C-terminal half of strand β2 (Gln37, Val39, Ala40, Arg41, Leu42), the loop connecting strands β2 and β3 (Asn45), two residues in strand β3 (Gln48 and Val49) and two residues in the helix (Ile58 and Tyr61). The three residues with the largest chemical shift perturbations ($\Delta_{H/N} \geq 80$ Hz) are His25 and Ala40, which are in direct contact with one another in the structure, and Val23. The location of the significantly perturbed residues on ribbon diagram and molecular surface representations of SDF-1α is shown in Figure 3(e). It can be seen that a contiguous, shallow, binding groove is formed principally comprising the top half of the solvent-exposed surface of the triple-stranded β-sheet, bounded on the left side by a small portion of the N-terminal loop and on the right-side by the exposed undersurface of the C-terminal helix. No perturbations were observed for resonances in the disordered N-terminal tail (residues 1–8). Since it is known that a peptide comprising residues 1–8 exhibits weak SDF-1 activity,[17] the current results suggest that the N terminus of SDF-1α, which is disordered in solution, possibly interacts with the second and/or third extracellular loops of CXCR4.

We attempted to further study the interaction of both CXCR4$^{1–27}$ and CXCR4$^{1–17}$ with ^{15}N/^{13}C-labeled SDF-1α by means of ^{13}C-separated/^{12}C-filtered NOE spectroscopy. Unfortunately, we were unable to detect any conclusive intermolecular NOEs, presumably due to significant line broadening of the interfacial side-chain resonances. Similar findings were previously reported for the interaction of the CC chemokine eotaxin with an equivalent peptide derived from its cognate receptor CCR3.[18]

It is of interest to compare the interaction surface mapped for SDF-1α binding to the N-terminal

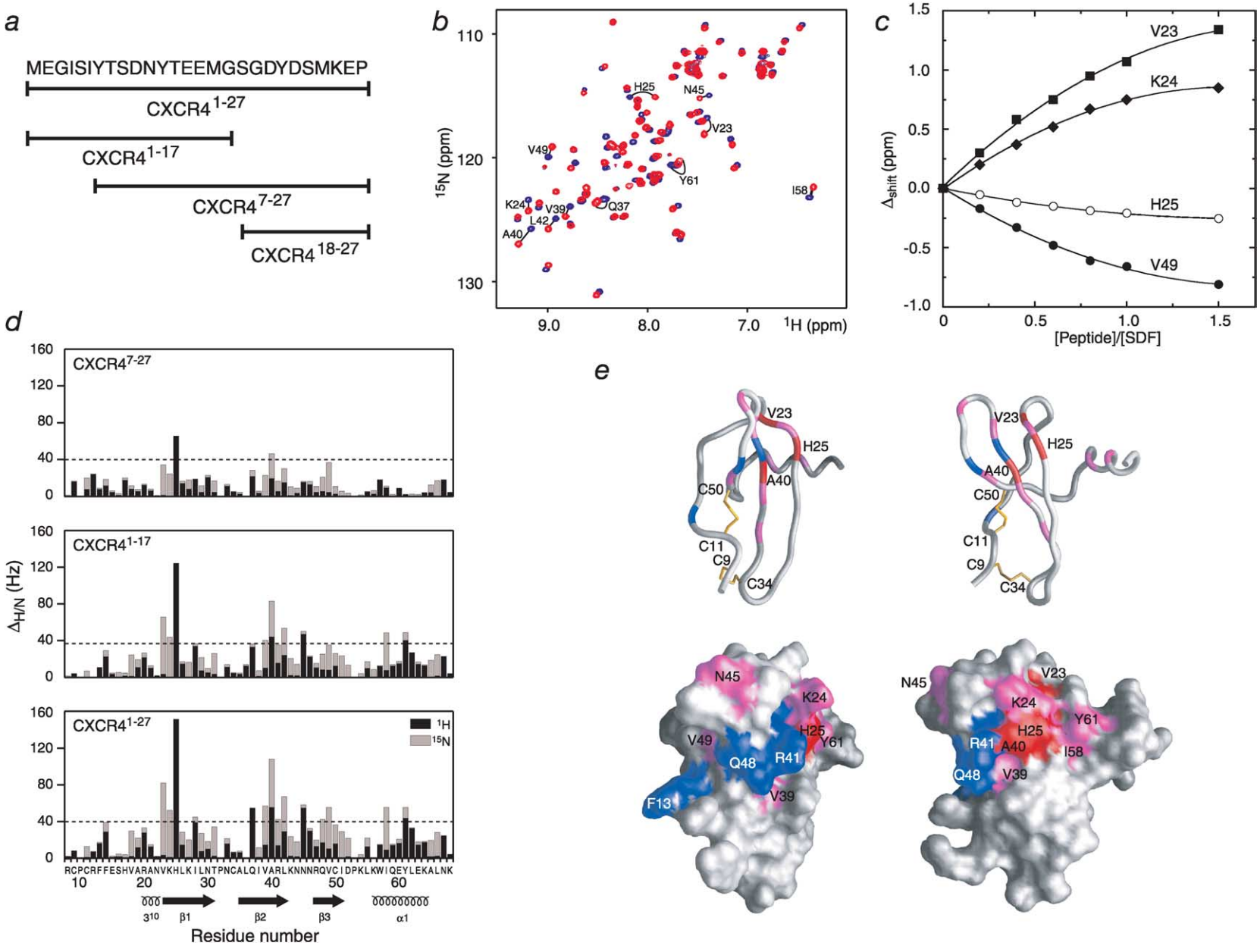

Figure 3 (*legend opposite*)

extracellular tail of CXCR4 with the interaction surfaces mapped for the chemokines interleukin-8 (a CXC chemokine),[19,20] eotaxin (a CC chemokine),[18] and fractalkine (CX_3C chemokine)[21] with peptides derived from the extracellular N-terminal tails of their respective receptors, CXCR-1, CCR3 and CX_3CR1. Similar binding affinities (in the range $K_D \sim 10$–150 μM) are observed for all four complexes. While not identical, the mapped interaction surfaces exhibit significant overlap. However, whereas the largest chemical shift perturbations observed for IL-8, eotaxin and fractalkine involve the N-terminal loop and strand β3 with no significant chemical pertubations observed within strand β1, the largest perturbations observed for SDF-1α involve strands β1 and β2 (Figure 3(d)).

In conclusion, we have resolved the discrepancy between the original NMR structure[4] and the X-ray structures[9,10] of SDF-1α and shown that the structure of monomeric SDF-1α in solution is essentially identical to that of the individual subunits of dimeric SDF-1α in the crystals. Using various peptides derived from the N-terminal extracellular tail of CXCR4 we have shown that the first six-residues of CXCR4 contribute significantly to binding. We have mapped the binding surface on SDF-1α for these peptides, and shown that the interaction surface overlaps with but is not identical to that observed for several other chemokines with equivalent peptides derived from their respective receptors.

Data bank accession codes

The coordinates and experimental restraints have been deposited in the Protein Data Bank (accession code 1VMC).

Acknowledgements

This work was supported by the AIDS Targeted Anti-viral Program of the Office of the Director of the National Institutes of Health (to G.M.C.).

References

1. Baggiolini, M. (2001). Chemokines in pathology and medicine. *J. Int. Med.* **250**, 91–104.
2. Tashiro, K., Tada, H., Heilker, R., Shirozu, M., Nakano, T. & Honjo, T. (1993). Signal sequence trap: a cloning strategy for secreted proteins and type I membrane proteins. *Science*, **261**, 600–603.
3. Nagasawa, T., Hirota, S., Tachibana, K., Takakura, N., Nishikawa, S.-I., Kitamura, Y. *et al*. (1996). Defects of B-cell lymphopoiesis and bone-marrow myelopoiesis in mice lacking the CXC chemokine PBSF/SDF-1. *Nature*, **382**, 6435–6638.
4. Crump, M. P. P., Gong, J.-H., Loetscher, P., Rajarathnam, K., Amara, A., Arenzana-Seisdedos, F. *et al*. (1997). Solution structure and basis for functional activity of stromal cell-derived factor-1: dissociation of CXCR4 activation from binding and inhibition of HIV-1. *EMBO J.* **16**, 6996–7007.
5. Bleul, C. C., Farzan, M., Choe, H., Parolin, C., Clark-Lewis, I., Sodroski, J. & Springer, T. A. (1996). The lymphocyte chemoattractant SDF-1 is a ligand for LESTR/fusin and blocks HIV-1 entry. *Nature*, **382**, 829–833.
6. Oberlin, E., Amara, A., Bachelerie, F., Bessia, C., Virelizier, J.-L., Seisdedos-Arenzana, F. *et al*. (1996). The CXC chemokine SDF-1 is the ligand for LESTR/fusin and prevents infection of T-cell-line-adapted HIV-1. *Nature*, **382**, 833–835.
7. Kucia, M., Jankowski, K., Reca, R., Wysoczynski, M., Bandura, L., Allendorf, D. J. *et al*. (2004). CXCR4-SDF-1 signaling, locomotion, chemotaxis and adhesion. *J. Mol. Histol.* **35**, 233–245.
8. Juarez, J. & Bendall, L. (2004). SDF-1 and CXCR4 in normal and malignant hematopoiesis. *Histol. Histopathol.* **19**, 299–309.
9. Dealwis, C., Fernandez, E. J., Thompson, D. A., Simon, R. J., Siani, M. A. & Lolis, E. (1998). Crystal structure of chemically synthesized [N33A] stromal cell-derived factor-1a, a potent ligand for the HIV-1 fusin coreceptor. *Proc. Natl Acad. Sci. USA*, **95**, 6941–6946.
10. Ohnishi, Y., Senda, T., Nandhagopal, N., Sugimoto, K., Shioda, T., Nagai, Y. & Mitsui, Y. (2000). Crystal structure of recombinant native SDF-1α with

Figure 3. Interaction of SDF-1α with peptides derived from the N-terminal extracellular tail of the CXCR4 receptor. (a) Sequences of the four overlapping peptides employed corresponding to residues 1–27, 1–17, 7–27 and 18–27 of CXCR4. (b) ^1H–^{15}N heteronuclear single quantum correlation spectra of SDF-1α free (red) and in the presence of 1.5 eq of $CXCR4^{1-27}$ (blue) in 50 mM phosphate buffer (pH 5.5). (c) Plot of chemical shift changes of the ^{15}N resonances of Val23, Lys24 and Val49 and the ^1HN resonance of His25 as a function of added $CXCR4^{1-27}$ peptide; the concentration of SDF-1α was 0.25 mM. The continuous curves represent best-fit theoretical curves to all the titration data simultaneously with an equilibrium dissociation constant of 45(±10) μM. (d) Combined $^1H/^{15}N$ chemical shift perturbation ($\Delta_{H/N}$ in Hz) at 600 MHz of SDF-1α upon complexation with $CXCR4^{1-27}$, $CXCR^{1-17}$ and $CXCR4^{7-27}$ given by $[(\Delta\delta^1H)^2+(\Delta\delta^{15}N)^2]^{1/2}$. (The partitioning of $\Delta_{H/N}$ into ^1H and ^{15}N contributions is indicated in the bar graph in black and gray, respectively.) The concentration of SDF-1α is 0.25 mM, and 1.5 eq of $CXCR4^{1-27}$, and 2 eq of $CXCR4^{1-17}$ and $CXCR4^{7-27}$ were employed. (All samples were maintained at pH 5.5). The broken line is drawn at $\Delta_{H/N}=40$ Hz. No chemical shift perturbation was observed upon addition of $CXCR4^{18-27}$. (e) Mapping of the largest chemical shift changes upon complexation with $CXCR4^{1-27}$ on the structure of SDF-1α displayed as tube (top) and molecular surface representations (bottom). Two approximately orthogonal views are displayed, and the views shown in the molecular surface representations correspond to those of the respective tube representations above; residues colored in red, lilac and blue have $\Delta_{H/N}$ values ≥80 Hz, 50–80 Hz, and 40–50 Hz, respectively; the gray surface indicates that there is no significant $^1H/^{15}N$ chemical shift perturbation ($\Delta_{H/N}<40$ Hz). The structure Figures were generated with the program GRASP.[32]

additional mutagenesis studies: an attempt at a more comprehensive interpretation of accumulated structure–activity relationship data. *J. Interferon Cytokine Res.* **20**, 691–700.
11. Clore, G. M. & Gronenborn, A. M. (1998). Determining structures of large proteins and protein complexes by NMR. *Trends Biotechnol.* **16**, 22–34.
12. Schwieters, C. D. & Clore, G. M. (2002). Reweighted atomic densities to represent ensembles of NMR structures. *J. Biomol. NMR*, **23**, 221–225.
13. Clore, G. M. & Kuszweski, J. (2002). χ1 rotamer populations and angles of mobile surface side chains are accurately predicted by a torsion angle database potential of mean force. *J. Am. Chem. Soc.* **124**, 2866–2867.
14. Grishaev, A. & Bax, A. (2004). An empirical backbone–backbone hydrogen-bonding potential in proteins and its applications to NMR structure refinement and validation. *J. Am. Chem. Soc.* **126**, 7281–7292.
15. Clore, G. M. & Gronenborn, A. M. (1995). Three-dimensional structures of α and β chemokines. *FASEB J.* **9**, 57–62.
16. Brelot, A., Heveker, N., Montes, M. & Alizon, M. (2000). Identification of residues of CXCR4 critical for human immunodeficiency virus coreceptor and chemokine receptor activities. *J. Biol. Chem.* **275**, 23736–23744.
17. Loetscher, P., Gong, J.-H., Dewald, B., Baggiolini, M. & Clark-Lewis, I. (1998). N-terminal peptides of stromal cell-derived factor-1 with CXC chemokine receptor 4 agonist and antagonist activities. *J. Biol. Chem.* **273**, 22279–22283.
18. Ye, J., Kobli, L. L. & Stone, M. J. (2000). Characterization of binding between the chemokine eotaxin and peptides derived from the chemokine receptor CCR3. *J. Biol. Chem.* **275**, 27250–27257.
19. Clubb, R. T., Omichinski, J. G., Clore, G. M. & Gronenborn, A. M. (1994). Mapping the binding surface of IL-8 complex with an N-terminal fragment of the type 1 human IL-8 receptor. *FEBS Letters*, **338**, 83–97.
20. Skelton, N. J., Quan, C., Reilly, D. & Lowman, H. (1999). Structure of a CXC chemokine-reeptor fragment in complex with interleukin-8. *Structure*, **7**, 157–168.
21. Mizoue, L. S., Bazan, J. F., Johnson, E. C. & Handel, T. M. (1999). Solution structure and dynamics of the CX_3C chemokine domain of fractalkine and its interaction with an N-terminal fragment of CX3CR1. *Biochemistry*, **38**, 1402–14414.
22. Garrett, D. S., Powers, R., Gronenborn, A. M. & Clore, G. M. (1991). A common sense approach to peak picking two-, three- and four-dimensional spectra using automatic computer analysis of contour diagrams. *J. Magn. Reson.* **95**, 214–220.
23. Bax, A., Vuister, G. W., Grzesiek, S., Delaglio, F., Wang, A. C., Tschudin, R. & Zhu, G. (1994). Measurement of homo- and heteronuclear J couplings from quantitative J correlation. *Methods Enzymol.* **239**, 79–105.
24. Bax, A., Kontaxis, G. & Tjandra, N. (2001). Dipolar couplings in macromolecular structure determination. *Methods Enzymol.* **339**, 127–174.
25. Cornilescu, G., Delaglio, F. & Bax, A. (1999). Protein backbone angle restraints from searching a database for chemical shift and sequence homology. *J. Biomol. NMR*, **13**, 289–302.
26. Clore, G. M. & Gronenborn, A. M. (1998). New methods of structure refinement for macromolecular structure determination by NMR. *Proc. Natl Acad. Sci. USA*, **95**, 5891–5898.
27. Schwieters, C. D. & Clore, G. M. (2001). Internal coordinates for molecular dynamics and minimization in structure determination and refinement. *J. Magn. Reson.* **152**, 288–302.
28. Schwieters, C. D., Kuszewski, J., Tjandra, N. & Clore, G. M. (2003). The Xplor-NIH NMR molecular structure determination package. *J. Magn. Reson.* **160**, 65–73.
29. Kuszewski, J., Gronenborn, A. M. & Clore, G. M. (1999). Improving the packing and accuracy of NMR structures with a pseudopotential for the radius of gyration. *J. Am. Chem. Soc.* **121**, 2337–2338.
30. Schwieters, C. D. & Clore, G. M. (2001). The VMD-XPLOR visualization package for NMR structure refinement. *J. Magn. Reson.* **149**, 239–244.
31. Carson, M. (1991). RIBBONS 4.0. *J. Appl. Crystallog.* **24**, 958–961.
32. Nicholls, A., Sharp, K. A. & Honig, B. (1991). Protein folding and association: insights into interfacial and thermodynamic properties of hydrocarbons. *Proteins: Struct. Funct. Genet.* **17**, 297–309.
33. Clore, G. M. & Garrett, D. S. (1999). R-factor, free R and complete cross-validation for dipolar coupling refinement of NMR structures. *J. Am. Chem. Soc.* **121**, 9008–9012.
34. Clore, G. M., Gronenborn, A. M. & Bax, A. (1998). A robust method for determining the magnitude of the fully asymmetric alignment tensor of oriented macromolecules in the absence of structural information. *J. Magn. Reson.* **133**, 216–221.
35. Laskowski, R. A., MacArthur, M. W., Moss, D. S. & Thornton, J. M. (1993). PROCHECK: a program to check the stereochemical quality of protein structures. *J. Appl. Crystallog.* **26**, 283–291.

Edited by M. F. Summers

(Received 23 September 2004; received in revised form 1 November 2004; accepted 2 November 2004)